

Modelling the effect of boundary scavenging on Thorium and Protactinium profiles in the ocean

M. Roy-Barman

▶ **To cite this version:**

M. Roy-Barman. Modelling the effect of boundary scavenging on Thorium and Protactinium profiles in the ocean. Biogeosciences, 2009, 6, pp.3091 - 3107. cea-02641299

HAL Id: cea-02641299
https://cea.hal.science/cea-02641299

Submitted on 28 May 2020

HAL is a multi-disciplinary open access archive for the deposit and dissemination of scientific research documents, whether they are published or not. The documents may come from teaching and research institutions in France or abroad, or from public or private research centers.

L'archive ouverte pluridisciplinaire **HAL**, est destinée au dépôt et à la diffusion de documents scientifiques de niveau recherche, publiés ou non, émanant des établissements d'enseignement et de recherche français ou étrangers, des laboratoires publics ou privés.



Distributed under a Creative Commons Attribution 4.0 International License

Biogeosciences, 6, 3091–3107, 2009
www.biogeosciences.net/6/3091/2009/
© Author(s) 2009. This work is distributed under
the Creative Commons Attribution 3.0 License.

Biogeosciences

Modelling the effect of boundary scavenging on Thorium and Protactinium profiles in the ocean

M. Roy-Barman

LSCE/IPSL Laboratoire CNRS/CEA/UVSQ, Domaine du CNRS, Bât 12 - avenue de la Terrasse, 91198 Gif-sur-Yvette Cedex, France

Received: 11 June 2009 – Published in Biogeosciences Discuss.: 31 July 2009
Revised: 15 November 2009 – Accepted: 18 November 2009 – Published: 18 December 2009

Abstract. The "boundary scavenging" box model is a cornerstone of our understanding of the particle-reactive radionuclide fluxes between the open ocean and the ocean margins. However, it does not describe the radionuclide profiles in the water column. Here, I present the transport-reaction equations for radionuclides transported vertically by reversible scavenging on settling particles and laterally by horizontal currents between the margin and the open ocean. Analytical solutions of these equations are compared with existing data. In the Pacific Ocean, the model produces "almost" linear ^{230}Th profiles (as observed in the data) despite lateral transport. However, omitting lateral transport biaises the ^{230}Th based particle flux estimates by as much as 50%. ^{231}Pa profiles are well reproduced in the whole water column of the Pacific Margin and from the surface down to 3000 m in the Pacific subtropical gyre. Enhanced bottom scavenging or inflow of ^{231}Pa-poor equatorial water may account for the model-data discrepancy below 3000 m. The lithogenic ^{232}Th is modelled using the same transport parameters as ^{230}Th but a different source function. The main source of the ^{232}Th scavenged in the open Pacific is advection from the ocean margin, whereas a net flux of ^{230}Th produced in the open Pacific is advected and scavenged at the margin, illustrating boundary exchange. In the Arctic Ocean, the model reproduces ^{230}Th measured profiles that the uni-dimensional scavenging model or the scavenging-ventilation model failed to explain. Moreover, if lateral transport is ignored, the ^{230}Th based particle settling speed may by underestimated by a factor 4 at the Arctic Ocean margin. The very low scavenging rate in the open Arctic Ocean combined with the enhanced scavenging at the margin accounts for the lack of high ^{231}Pa/^{230}Th ratio in arctic sediments.



Correspondence to: M. Roy-Barman
(matthieu.roy-barman@lsce.ipsl.fr)

1 Introduction

^{230}Th and ^{231}Pa are important oceanic tracers of marine particles and deep water circulations. ^{230}Th and ^{231}Pa are both produced uniformly in the ocean by radioactive decay of uranium isotopes (^{234}U and ^{235}U respectively) and they are both scavenged rapidly on marine particles that transport them towards the sediment on a time scale of 20 y for ^{230}Th and of 200 y for ^{231}Pa. In absence of lateral transport by currents, particulate transport balances in situ production. In this case, the vertical profiles of ^{230}Th and ^{231}Pa are expected to increase linearly with depth, as predicted by the uni-dimensional ("1-D") reversible scavenging model (Bacon and Anderson, 1982). Deviations from a linear profile indicate that oceanic currents carry significant amounts of ^{230}Th and ^{231}Pa away from their production site (Coppola et al., 2006; Roy-Barman et al., 2002; Rutgers van der Loeff and Berger, 1993). The early study of ^{230}Th in the ocean revealed linear increase of dissolved ^{230}Th with depth in agreement with the balance between the in situ production and the reversible scavenging of ^{230}Th on sinking particles (Bacon and Anderson, 1982; Nozaki et al., 1981). Further works have stressed that a significant fraction of dissolved ^{231}Pa and at least some dissolved ^{230}Th could be exported from area of low particle flux to area with high particle flux where ^{230}Th and ^{231}Pa are efficiently scavenged to the sediment (Anderson et al., 1983). This process is called "boundary scavenging" because ocean boundaries/margins are generally places with high particle concentration and sedimentation rates (particle flux effect) and where the particulate matter chemistry is such that it has a higher affinity for Pa compared to the open ocean (particle chemistry effect). The concept of boundary scavenging was first applied to horizontal transport of ^{210}Pb toward lateral ocean boundaries (Bacon, 1977; Spencer et al., 1981). The effect of the lateral transport on particulate flux of ^{230}Th and ^{231}Pa was quantified with box modelling, hereafter referred as boundary scavenging

Published by Copernicus Publications on behalf of the European Geosciences Union.

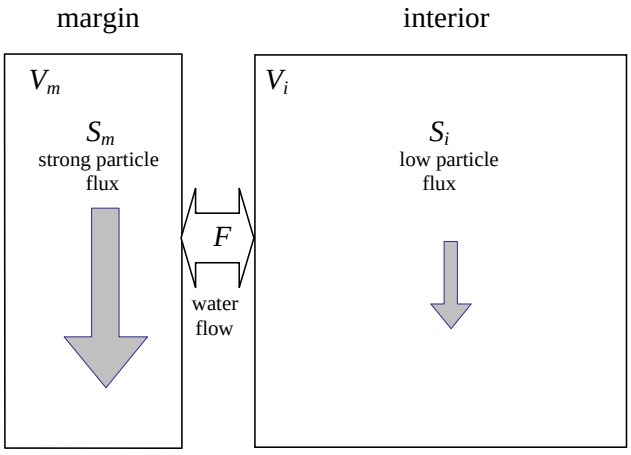


Fig. 1. Principle of the boundary scavenging profile model.

box model (Anderson et al., 1983; Bacon, 1988; Bacon et al., 1985). More than 25 years later, this model is still the cornerstone of our understanding of the distribution of the particle reactive element fluxes between the margins and the open ocean. In this box model, only the depth-averaged concentrations of Pa and Th are considered, but the water column profiles are not modelled. Nevertheless, it was noted that the greater sensitivity of ^{231}Pa to boundary scavenging compared to ^{230}Th could account for its constant concentration in the deep water as opposed to the linear increase of ^{230}Th (Nozaki and Nakanishi, 1985). As a consequence, despite the potential influence of boundary scavenging in most oceanic regions, the 1-D reversible scavenging model is widely used to discuss ^{230}Th water column data and determine particle settling velocities including in ocean margins, as long as there is no obvious evidence of ventilation or upwelling. However, a recent study of the particle dynamics on the Kerguelen plateau stressed on the importance of taking into account horizontal advection of the open ocean water to evaluate the particles flux with the dissolved and particulate ^{230}Th profiles (Venchiarutti et al., 2008).

Here, I model the water column profiles of ^{230}Th, ^{232}Th and ^{231}Pa corresponding to the 2 box ocean (ocean margin and ocean interior) proposed by (Bacon, 1988) or more generally when 2 areas with distinct scavenging conditions exchange water. I use the simple approach of (Rutgers van der Loeff and Berger, 1993) and (Venchiarutti et al., 2008) to obtain analytical solutions of the transport equations. Then, I compare the results with some existing data to discuss the shape of the Th-Pa profiles and the evaluation of the particle flux with ^{230}Th profiles.

2 The boundary scavenging profile model

2.1 Boxes and water transport

The ocean is divided in 2 boxes: the ocean margin and the ocean interior (Fig. 1). The volumes of the margin and of the ocean interior are V_m and V_i (m^3). These 2 boxes exchange a total flux of water F (m^3/s). For simplicity, I assume that the water flows horizontally between the boxes (this is true if isopycnal surfaces are essentially horizontal) and that this flux is homogeneously distributed throughout the water column (a similar hypothesis is done by Rutgers van der Loeff and Berger, 1993). The vertical eddy diffusion is neglected in the surface mixed layer (see Sect. 2.4) and in the deep waters (see Sect. 3.1.1). Neglecting vertical mixing within each box implies that ventilation of deep layers by lateral exchange with Polar Regions is also neglected (this point will be justified for the North Pacific Ocean in Sect. 3.1.1 and the Arctic Ocean in Sect. 3.2.1). It follows that at any depth the residence time of the water is $\tau_m = V_m/F$ in the margin and $\tau_i = V_i/F$ in the ocean interior. Keeping constant τ_m and F values with depth implicitly implies the crude approximation that the ocean margin has a flat bottom bathymetry (Fig. 1) rather than a deepening slope. It must be noted that each box is assumed to be well mixed horizontally so that concentration gradients exist just between the boxes, not within boxes. It implies that the nuclide distribution should be represented by an average profile rather than by a single profile. As discussed in Sect. 3.1.3, using an "extreme" profiles (e.g. a profile sampled in the centre of the gyre) rather than an average profile over the box (average profile over the gyre if available) will lead to somewhat different estimates of the mixing time that reflect the strong isolation of the gyre centre from the margin compared to the whole gyre.

2.2 Particle flux

Particles are assumed to be produced at the sea surface (z=0). Then, particles settle at constant velocity: S_m for the margin and S_i for the ocean interior. These settling velocities represent the mean settling velocity of small particles defined operationally as the particles collected on filters with porosity ranging from 0.2 to 1 μm. This average settling velocity of the fine particle integrates multiple processes including aggregation of small particles on large rapidly sinking particles and desegregation that are not explicitly represented in the model. The particle concentration is also not explicitly considered here. The particle concentration is embedded in the dissolved-particulate partition coefficient K introduced in the next section.

I also assume that the constant particle flux is not perturbed by lateral transport of particles from one oceanic reservoir to the other. This is justified because, for transport at the ocean basin scale, marine particles settle through the entire water column fast enough that they do not have time to be

advected far from their region of origin before they reach the seafloor (Henderson et al., 1999; Siddall et al., 2005). It is also consistent with the idea that particle dynamics in the water column is strongly driven by surface parameters such as biological productivity in the local surface water (high settling speed of particles in productive area, low settling speed of particles in oligotrophic areas).

The treatment of the particle transport is simplistic compared to the complexity of the real particle dynamics. The aim is to use the same particle dynamics as the 1-D reversible scavenging model (Bacon and Anderson, 1982; Nozaki et al., 1981) in order to restrict the investigation to the effect of lateral transport on radionuclide distribution.

2.3 Tracer transport

In each box, ^{230}Th (as well as ^{231}Pa) is produced by in situ decay of U at a constant rate P, it is transported toward the sea floor by reversible scavenging on sinking particles and it is transported horizontally by the water flow. Considering the long half-life of ^{230}Th (75 000 y) and ^{231}Pa (32 500 y), the radioactive decay of these isotopes is neglected. Dissolved and particulate concentrations are noted C_d^m and C_p^m for the margin and C_d^i and C_p^i for the ocean interior.

The total quantity of tracer (dissolved + particulate) is transported horizontally from one reservoir to the other (Siddall et al., 2005). The conservation equation of total ^{230}Th (or ^{231}Pa) is given by:
for the ocean margin:

$$\frac{d(C_d^m+C_p^m)}{dt} = -S_m\frac{dC_p^m}{dz} + P + \frac{F}{V_m}\left[(C_d^i+C_p^i)-(C_d^m+C_p^m)\right] \quad (1a)$$

for the inner ocean:

$$\frac{d(C_d^i+C_p^i)}{dt} = -S_i\frac{dC_p^i}{dz} + P + \frac{F}{V_i}\left[(C_d^m+C_p^m)-(C_d^i+C_p^i)\right] \quad (1b)$$

In the right member of these equations, the first term represents the vertical particulate transport, the second term represents the in situ production and the third term corresponds to the lateral transport. To solve these equations, the relation between C_p and C_d need to be specified. The dissolved and particulate pools exchange material through adsorption and desorption. If these processes are fast enough, it can be assumed that there is a chemical equilibrium between the dissolved and the particulate pool (Bacon and Anderson, 1982; Nozaki et al., 1981; Roy-Barman et al., 1996):

$$C_p^m = K_m C_d^m \quad (2a)$$

$$C_p^i = K_i C_d^i \quad (2b)$$

K represents the apparent partition coefficient of Th between the dissolved and the particulate phase with C_p expressed as g of Th per litre of filtered seawater. These relations express a fast reversible equilibrium between dissolved and particulate thorium. This is the assumption used in the 1-D model and the scavenging–mixing model to represent the dissolved-particulate relationship (Bacon and Anderson, 1982; Coppola et al., 2006; Moran et al., 2002; Nozaki et al., 1981; Roy-Barman et al., 1996, 2002; Rutgers van der Loeff and Berger, 1993). The determination of the partition coefficient of Pa and Th between the various particle types is still a matter of debate (Chase et al., 2002; Santschi et al. 2006; Roy-Barman et al., 2005, 2009). This is why I did not try to represent particles of different chemical composition with specific K but I rather used a bulk partition coefficient. In the following, K is assumed to be constant with depth for both Th and Pa, as also assumed in the 1-D model and the scavenging-mixing model. This may be questionable as, for example, degradation and dissolution of biogenic particles causes the abundance and composition of particles to vary with depth. A significant dissolution of Th bearing phases would produce a non-linear profile that is not consistent with observations (Roy-Barman et al., 1996). Pa is preferentially scavenged by biogenic silica that is known to experience dissolution through the water column (Scholten et al., 2008). However, the accelerated increase of dissolved ^{231}Pa with depth that could be expected (based on the analysis of ^{230}Th distribution by Roy-Barman et al., 1996) does not appear clearly in the data (Nozaki and Nakanishi, 1985; Bacon et al., 1989).

2.4 Solving the equilibrium model

Assuming that each reservoir is at steady state and introducing the reversible equilibrium between dissolved and particulate thoriumin (Eq. 1a and b), it follows that:

$$-S_m K_m\frac{dC_d^m}{dz} + P + \frac{F}{V_m}\left[(1+K_i)C_d^i-(1+K_m)C_d^m\right] = 0 \quad (3a)$$

for the inner ocean:

$$-S_i K_i\frac{dC_d^i}{dz} + P + \frac{F}{V_i}\left[(1+K_m)C_d^m-(1+K_i)C_d^i\right] = 0 \quad (3b)$$

First I consider only the in situ produced ^{230}Th (also called ^{230}Th$_{xs}$). If the effect of the mixed layer is neglected (Roy-Barman et al., 1996), the amount ^{230}Th produced at z=0 in an infinitely thin layer tends towards 0, so that in this layer, marine particles have not accumulated ^{230}Th. It follows 2 boundary conditions: C_p^m=0 and C_p^i=0. It implies that C_d^m=C_p^m/K_m=0 and C_d^i=C_p^i/K_i=0.

Under these conditions, the solutions of Eq. (3a) and (3b) are (see Appendix A):

$$C_d^i = \frac{\sigma_\infty}{(1+K_i)}\times z + \left(\frac{P}{S_i K_i}-\frac{\sigma_\infty}{(1+K_i)}\right)\times z_0\times\left(1-e^{-\left(\frac{z}{z_0}\right)}\right) \quad (4a)$$

$$C_d^m = \frac{\sigma_\infty}{(1+K_m)}\times z + \left(\frac{P}{S_m K_m}-\frac{\sigma_\infty}{(1+K_m)}\right)\times z_0\times\left(1-e^{-\left(\frac{z}{z_0}\right)}\right) \quad (4b)$$

with

$$z_0 = \left(\frac{F}{V_i} \frac{(1+K_i)}{S_i K_i} + \frac{F}{V_m} \frac{(1+K_m)}{S_m K_m} \right)^{-1} \quad (5)$$

and

$$\sigma_\infty = \frac{P(V_m + V_i)}{\frac{S_m K_m V_m}{(1+K_m)} + \frac{S_i V_i K_i}{(1+K_i)}} \quad (6)$$

z_0 is the depth below which lateral mixing becomes significant compared to particulate transport. σ_∞ represents the slope of the total (dissolved + particulate) ^{230}Th concentration depth profiles at great depth ($z \gg z_0$) in the margin and the inner ocean. Equation (4a) and (4b) are converted to the total quantity of ^{230}Th as follow:

$$C_t^i = \sigma_\infty \times z + (\sigma_i - \sigma_\infty) \times z_0 \times \left(1 - e^{-\left(\frac{z}{z_0}\right)} \right) \quad (7a)$$

$$C_t^m = \sigma_\infty \times z + (\sigma_m - \sigma_\infty) \times z_0 \times \left(1 - e^{-\left(\frac{z}{z_0}\right)} \right) \quad (7b)$$

where $\sigma_m = (1+K_m) \times P/(S_m K_m)$ and $\sigma_i = (1+K_i) \times P/(S_i K_i)$ represent the slopes of the total (dissolved + particulate) ^{230}Th concentration depth profiles that would be observed in the margin and the inner ocean if there was no lateral mixing (F=0). In the following, these equations will be referred as "the boundary scavenging profile model".

3 Discussion

The model will be compared with existing data from the Pacific Ocean and the Arctic Ocean. The Pacific Ocean is the largest ocean so that margin-interior interactions should occur on a relatively long time scale. The Arctic Ocean is smaller than the Pacific. It is the ocean with the largest proportion of shelves and marginal seas whereas the inner ocean is permanently covered by sea-ice, producing a very strong biogeochemical contrast between the margin and the inner ocean. I do not try to compare directly the model with Atlantic Ocean data because the strong ventilation of the deep waters strongly influences the shape of the Pa and Th profiles. However, implications of the model for the Atlantic Ocean will be discussed.

3.1 North Pacific Ocean

3.1.1 ^{230} Th

I focus on the North Pacific Ocean because it covers most available data in the Pacific Ocean. The margin-inner ocean limit is set at the 4000 m isobath. The water residence times used by (Bacon, 1988) were: τ_i=460 y, τ_m=140 y. The dense waters formed in the North Pacific flow as intermediate water above 1000 m, while denser waters of the North Pacific are dominated by the inflow from the South Pacific (Reid, 1997). In the Central North Pacific, were ^{230}Th scavenging is particularly slow (Roy-Barman et al., 1996), CFC-ages of recently ventilated waters (~0–1000 m in the thermocline) are approximately 4 times larger than the ^{230}Th scavenging residence time calculated at the same depth, indicating that ^{230}Th transport is dominated by the reversible scavenging rather than by water ventilation (Fine et al., 2001; Boyle et al., 2005). In addition, it must be kept in mind that CFC-ages may be strongly biased toward young ages due to water mass mixing. Therefore, it is likely that ^{230}Th profiles are not strongly affected by the thermocline ventilation in the North Pacific Ocean. The effect of ventilation is certainly stronger for ^{231}Pa that has a longer scavenging residence time although it is not possible to quantify it clearly.

A profile obtained in the NW Pacific Ocean (AN5: 40°00′ N, 145°28′ E) is used as reference for the Pacific Ocean margin (Nozaki and Yang, 1987). It was preferred to discrete Pa and Th data collected less than 50 miles off the slope of the Shikoku Basin because they form a very scattered profile (possibly due to local effects) that corresponds on average to the AN5 profile (Nozaki and Yang, 1987). The inner ocean is represented by the HOT station (22°45′ N, 158° W, ~100 km north of Oahu) in the Central North Pacific Ocean (Roy-Barman et al., 1996). Knowing the concentration profiles and K values from field data, the settling speeds are adjusted to obtain a good agreement with the reference profiles (Table 1, Fig. 2).

The modelled profiles are close to, but not exactly, strait lines (Fig. 2a). At the ocean margin, where scavenging is intense, the deep ^{230}Th concentration is slightly higher than what it would be if no lateral mixing occurred. Conversely, in the inner ocean, the modelled profile exhibit slightly lower concentrations than if no advection occurred. This is because some ^{230}Th is transported from the low particle flux region to the high particle flux region ("particle flux effect").

Above ~1500 m, the boundary scavenging profiles are almost identical to the 1-D scavenging profiles. Indeed, if $z \gg z_0$ (Appendix B, Eq. B6a and b)

$$C_d^i \approx \frac{P}{S_i K_i} \times z \quad (8a)$$

$$C_d^m \approx \frac{P}{S_m K_m} \times z \quad (8b)$$

Close to the surface or/and if the water residence time is very long in the inner ocean and in the margin, the effect of lateral transport is negligible and the profiles are identical to those expected without advection. As a consequence, the settling speed of marine particles must be determined with ^{230}Th data collected in the upper part of the water column because they are less likely to be affected by boundary scavenging.

At z=0, the boundary condition implies that the ^{230}Th$_d$ concentration is equal to zero (no mixed layer). It introduces a small discrepancy with the data. The ^{230}Th concentration over the mixed layer of depth h is constant and equal to the

Table 1. Parameters of the boundary scavenging profile model.

	Pacific 1 (slow mixing)		Pacific 2 (fast mixing)		Arctic 1	
	inner ocean	ocean margin	inner ocean	ocean margin	inner ocean	ocean margin
Circulation						
V (m^3)[a]	1.64×10^{17}	5×10^{16}	1.64×10^{17}	5×10^{16}	6.5×10^{15}	1.5×10^{15}
F (m^3/y)[b]	3.57×10^{14}	3.57×10^{14}	1.1×10^{15}	1.1×10^{15}	1.3×10^{14}	1.3×10^{14}
$\tau(y)$	460	140	150	45.8	50	11.5
particles						
S (m/y)[c]	370	500	330	700	150	1500
Thorium						
P_{Th} (fg/m^3/y)[d]	540	540	540	540	540	540
K^e_{Th}	0.15	0.3	0.15	0.3	0.06	0.30
z_{0Th} (km)[f]	9.3	9.3	3.2	3.2	0.38	0.38
Particulate ^{230}Th flux/ overlying production (depth)[f]	95% (4000 m)	115% (4000 m)	85% (4000 m)	148% (4000 m)	29% (2000 m)	409% (2000 m)
Protactinium						
P_{Pa} (fg/m^3/y)[d]	25	25	25	25	25	25
K^e_{Pa}	0.015	0.15	0.015	0.15	0.006	0.1
z_{0Pa} (km)[f]	2.0	2.0	0.6	0.6	0.043	0.043
Particulate ^{231}Pa flux at depth/overlying production[f]	59% (4000 m)	235% (4000 m)	25% (4000 m)	316% (4000 m)	6% (2000 m)	509% (2000 m)
F=$(Th/Pa)_p/(Th/Pa)_d$ = (K^{Th}/K^{Pa})[f]	10	2	10	2	10	3
$(Pa/Th)_p/(P_{Pa}/P_{Th})$[f]	0.62 (4000 m)	2.0 (4000 m)	0.40 (4000 m)	2.1 (4000 m)	0.2 (2000 m)	1.2 (2000 m)

[a] Pacific data from Bacon (1988). Arctic data from Jakobsson (2002).
[b] Pacific data from Bacon (1988); Matsumoto (2007); Owens and Warren (2001). Arctic data from Carmack et al. (1995).
[c] values derived in this paper by fitting the modelled ^{230}Th profiles to measured ^{230}Th profiles: Pacific profiles from Roy-Barman et al. (1996); Nozaki and Yang (1987); Arctic profiles: Bacon et al. (1989); Cochran et al. (1995); Edmonds et al. (1998).
[d] Anderson et al. (1983).
[e] Pacific data from Anderson et al. (1983); Nozaki and Nakanishi (1985); Nozaki et al. (1987, 1995); Roy-Barman et al. (1996). Arctic data from Bacon et al. (1989); Cochran et al. (1995); Moran et al. (2005); Scholten et al. (1995).
[f] values deduced from the other parameters.

concentration expected at the depth h with the 1-D model if there was no vertical mixing (Roy-Barman et al. 1996). Hence the effect of the mixed layer on the real profile will be limited to the very surface sample(s) and it can be neglected for the purpose of this article where the discussion concerns mostly the deep profile.

At 4000 m, the ^{230}Th particulate flux ($S \times C_p$) represents 115% of the in situ production in the overlying water column at the margin and 95% of the in situ production in the overlying water column in the inner ocean. Thus, the contrast between the margin and the inner ocean is relatively weak compared to the estimates based on a GCM (Henderson et al., 1999). If lateral mixing is ignored, the 1-D reversible model overestimates the settling speed of particles by ∼5% in the inner ocean and underestimated it by ∼16% in the margin. In this particular case, the difference between the advection-mixing model and the 1-D model are relatively small because the water residence time in each reservoir is long compared to the scavenging residence time (Table 1).

However, Bacon (1988) suggested that the relatively long water residence time that he estimated with his box model and data available at the time could be overestimated by a factor 2 to 3 due to the paucity of Pa and Th water column data. Therefore, the water residence time is re-evaluated using recent data independently of thorium data and boundary scavenging models.

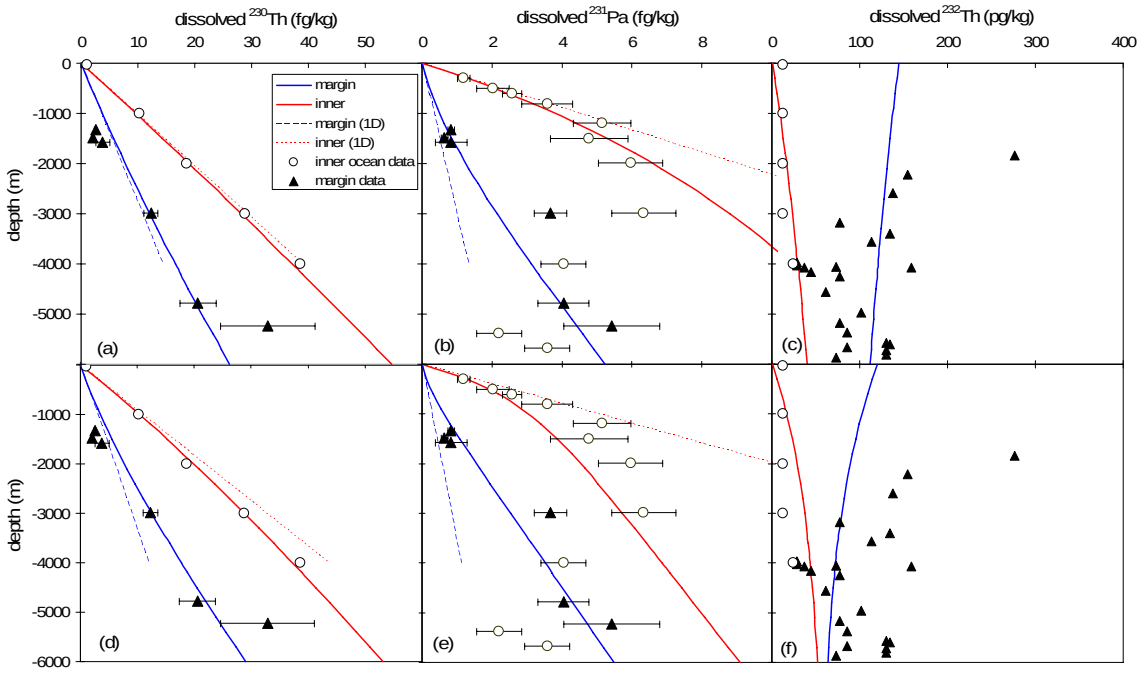


Fig. 2. Modelled profiles and comparison with data for the North Pacific Ocean. **(a)** to **(c)**: Pacific 1 simulation (slow mixing). **(d)** to **(f)**: Pacific 2 simulation (fast mixing). See Table 1 for model parameters. "1-D" curves are obtained for the ocean margin and the inner ocean by setting F=0 and keeping all the other parameters identical.

A recent synthesis of the $\Delta^{14}C$ collected during the WOCE program suggests that the mixing time of the deep water between the ocean margin and inner North Pacific is of the order of 100–200 y (Matsumoto, 2007). This mixing time is different from the more familiar absolute age and ventilation age that is of the order of 1000 y (see Matsumoto, 2007, for discussion).

Isopycnal diffusion contribution to margin-open ocean mixing can be evaluated as follows: for a length scale Δx=5000 km (the distance between the centre of the inner ocean and the margin), the horizontal eddy diffusion coefficient K_H is of the order of 2–6$\times 10^7$ cm^2/s in the deep ocean (Ledwell et al., 1998, Sarmiento et al., 1982), the time scale Δt necessary to achieve diffusion is

$$\Delta t = \frac{(\Delta x)^2}{2 \times K_H} \quad (9)$$

The above K_H values are on the high end of those used in Ocean General Circulation Models to parametrize horizontal eddy diffusion. This is because natural or artificial tracer dispersion integrates also the effect of the large scale circulation. With the above values, we obtain Δt=70–200 y which is in the same range as the ^{14}C estimates. Based on the ^{14}C and the isopycnal diffusion estimates, I choose a residence time of 150 y for the inner deep North Pacific. With a 3.2 to 1 ratio between the inner ocean and the margin (Bacon, 1988), the water residence time in the margin is of the order of 50 y. This residence time is consistent with the strong currents ($\sim 24 \times 10^6$ m^3/s below 2000 m) flowing along the Japan slope (Owens and Warren, 2001).

Using these new residence times, it is necessary to increase the S_m and to decrease S_i to maintain the same concentration gradient with a more vigorous horizontal mixing. Therefore, the deviation between the 1-D and the boundary scavenging profile model increases. At 4000 m the ^{230}Th particulate flux ($S \times C_p$) represents 148% of the in situ production in the overlying water column at the margin and 86% of the in situ production in the overlying water column in the inner ocean. The scavenging contrast between the margin and the inner ocean become closer to the estimates based on a GCM (Henderson et al., 1999). If lateral mixing is ignored so that the 1-D scavenging model is used to determine the settling speed of particles, the settling speed of particles will be overestimated by ~14% in the inner ocean and underestimated by ~30% (48%/148%) at the margin.

Finally, it must be noted that vertical (diapicnal) eddy diffusion in the deep ocean cannot account for the curvature of the profile. Using a typical vertical eddy diffusion coefficient in the deep ocean K_z=1 cm^2/s (Munk, 1966; Thorpe, 2004) for the whole water column and assuming no diffusion of ^{230}Th from the sediment, it appears that the curvature of the profile due to the vertical eddy diffusivity is restricted within ~100 m above the seafloor (Roy-Barman et al., 1996). For ^{231}Pa that will be presented in the next section and that is 10 times les particle reactive than ^{230}Th, the curvature of the profile due to the vertical eddy diffusivity is restricted within

$\sim$500 m above the seafloor. Higher, K_z value (>1 cm^2/s) occurs in the deep ocean but they are restricted very close to the bottom topography (Ledwell et al., 2000), limiting its effect on the Th or Pa profile to the seafloor vicinity. In addition, it must be noted that isopycnal diffusion along slopping isopycnal surfaces probably accounts for most of the vertical eddy diffusivity in the deep ocean (Sarmiento and Rooth, 1980).

3.1.2 ^{231} Pa

I now apply the boundary scavenging profile model to ^{231}Pa. The water residence time, the settling speed of particles and the boundary conditions remain unchanged compared to simulation (1), the only changes concern K_i and K_m due to the different chemical behaviour of Pa and Th. According to literature data (Table 1), $K_i^{Pa} \approx K_i^{Th}/10$ in the inner ocean and $K_m^{Pa} \approx K_m^{Th}/2$ in the ocean margin (Anderson et al., 1983; Nozaki and Nakanishi, 1985; Nozaki et al., 1987, 1995). The main features of the modelled ^{230}Th profiles also occur for the modelled ^{231}Pa profiles:

- in the deep ocean, the modelled ^{231}Pa concentration at the margin is higher and the modelled ^{231}Pa concentration in the inner ocean is lower than if no lateral mixing occurred (F=0).
- very close to the surface, the advection-scavenging profiles are almost identical to the 1-D scavenging profiles. It occurs only above $\sim$300 m (compared to 1500 m for ^{230}Th) because ^{231}Pa much more sensitive to lateral mixing than ^{230}Th.

At great depth (below z_0), the "margin" and "inner ocean" ^{231}Pa modelled profiles tend to be parallel. z_0 is the depth where the 2 profiles start to be parallel due to horizontal mixing of ^{231}Pa. The concentrations remain different because above z_0 an excess of ^{231}Pa has built up in the open ocean due to a lower scavenging rate. This excess is transported at greater depth by reversible scavenging on sinking particles. Strictly speaking, it is the slopes of the total concentration profiles that tend toward the same value (Appendix B, Eq. B8a and b).

The difference of concentration between the 2 profiles is equal to 2.5 fg/l (we neglect particulate Pa that represents a small fraction of the total). This concentration difference is the result of ^{231}Pa ingrowth when a ^{231}Pa-depleted water mass leaves the margin (where scavenging is more intense), and stays in the inner ocean (where the scavenging rate is much lower). Dividing this concentration difference by the production rate of ^{231}Pa (0.025 fg/l/y) yields a time difference of 100 y. This time difference is lower than the water residence time in the inner ocean (150 y) because some ^{231}Pa is scavenged in the inner ocean even if it is less effective than at the margin (Appendix B, Eq. B13).

These theoretical curves are compared with the AN5 profile (margin) and with the Ce-8 profile (12.75° N, 173.23° W)(Nozaki and Nakanishi, 1985) because ^{231}Pa data are not available at the HOT Station. The Ce-8 profile is also sampled in the subtropical gyre and it has a ^{230}Th profile very similar to the HOT station (but with less accurate data). Particulate ^{231}Pa is not available but it generally represents less than 5% of the total ^{231}Pa. With the "Pacific 2" set of parameters (Table 1), the model correctly reproduces the margin profile down to 6000 m. It correctly reproduces the inner ocean profile between the surface and $\sim$3000 m (Fig. 2e). The model fails to reproduce the lower part of the inner ocean profile where the concentration remains constant with depth and becomes close to the margin profile.

It must be noted that the subtropical gyre profiles are located in area with a seafloor depth of 6000 m, but close to high relief with seafloor depth of 4000 m such as the Gilbert Ridge. Therefore, the circulation of the deep waters found at station Ce8 along the Gilbert ridge (Yanagimoto and Kawabe, 2007) may have enhanced locally the scavenging of ^{231}Pa (as it can be seen also for ^{230}Th). In addition, these waters flowing from the south may have been stripped from their ^{231}Pa in the equatorial Pacific by the enhanced siliceous particulate flux. We also note that very low ^{231}Pa concentrations were measured on the eastern margin of the Pacific Ocean (Anderson et al., 1983). Obviously, more data are required to further constrain this point.

3.1.3 From boundary scavenging to boundary exchange

Until now, only in situ produced nuclides have been discussed. I now consider the case of ^{232}Th that is derived from continental inputs. Dissolved ^{232}Th is produced by dissolution of lithogenic material. The main source of lithogenic particulate matter in the ocean is the river input in the coastal ocean (Table 2). It represents approximately 10 times the total atmospheric input. The flux of lithogenic aerosols at the margin is approximately 100 times higher than in the open ocean.

The average ^{232}Th content in lithogenic particles is of the order of 10 ppm. Φ_m and Φ_I are the fluxes of ^{232}Th released by dissolution of the incoming particles at the margin and in the inner ocean, assuming 1% of dissolution for both riverine and atmospheric particles (Arraes-Mescoff et al., 2001; Roy-Barman et al., 2002). For S_i, S_m, K_i and K_m parameter, I use the same values as for ^{230}Th because isotopes of the same element are expected to have the same chemical behaviour in solution. The distribution of the dissolved ^{232}Th concentration with depth is then given by (Appendix A, Eq. A27a and b):

$$C_d^i = \left(\frac{(1+K_m)\Phi_m}{K_m S_m} - \frac{(1+K_i)\Phi_i}{K_i S_i}\right)\frac{F}{S_i V_i K_i} \times z_0 \times \left(1 - e^{-\left(\frac{z}{z_0}\right)}\right) + \frac{\Phi_i}{K_i S_i} \quad (10a)$$

$$C_d^m = \left(\frac{(1+K_i)\Phi_i}{K_i S_i} - \frac{(1+K_m)\Phi_m}{K_m S_m}\right)\frac{F}{S_m V_m K_m}$$

Table 2. Lithogenic flux to the North Pacific Ocean.

	Lithogenic material flux (10^{12} g/y)	^{232}Th flux released by dissolution**** (10^6 pg/m^2/y)	Nd flux released by dissolution**** (10^6 pg/m^2/y)
Whole North Pacific atmospheric flux	480*	1.6	4.8
Central North Pacific atmospheric flux	20**	0.067	0.2
lithogenic flux by river discharge	6000***	33	100

* Uematsu et al. (1985); ** Duce et al. (1991); *** Milliman and Meade (1983); **** assuming 1% dissolution of lithogenic matter and considering that the North Pacific surface is 89×10^{12} m^2.

$$\times z_0 \times \left(1-e^{-\left(\frac{z}{z_0}\right)}\right)+\frac{\Phi_m}{K_m S_m} \quad (10b)$$

The modelled profiles are compared to the HOT profile (inner ocean) and to the compilation of Western Pacific margin data as dissolved ^{232}Th concentration is not available at station AN-5 (Nozaki and Yang, 1987). The modelled profiles do not reproduce precisely the data (Fig. 2c and f), but they account for several important features: increasing ^{232}Th concentration with depth in the open ocean and decreasing ^{232}Th concentration with depth in the ocean margin. If there was no water exchange between the open ocean and the margin (F=0 in Eq. 10a and b), both profiles should exhibit constant concentration with depth (Roy-Barman et al., 1996). In the open ocean, the increase of ^{232}Th concentration with depth is due to advection of ^{232}Th -rich coastal water. At the ocean margin, the decrease ^{232}Th concentration with depth is due to the progressive flushing of the ^{232}Th-rich margin water by ^{232}Th-poor open ocean deep water.

A low water mixing rate allows a larger concentration difference between the open ocean and the ocean margin. However, it reduces the vertical concentration gradient in each reservoir. Given the limited ^{232}Th data set, the ^{232}Th concentration is much more sensitive to the water circulation pattern than uniformly in situ produced ^{230}Th. The very low ^{232}Th content at the HOT station may be due to the reduced inflow of margin water to the centre of the gyre compared to the average open ocean (modelled reservoir). This would be consistent with the perfectly linear ^{230}Th profile that is not perfectly reproduced by the slightly curved ^{230}Th modelled profile of the Pacific 2 data set (Table 1, Fig. 2d).

Given that Φ_i is 2 orders of magnitude smaller than Φ_m, setting Φ_i=0 does not change the modelled ^{232}Th profile of the inner ocean significantly (not shown). This means that most ^{232}Th in the inner ocean is advected from the ocean margin. Hence, the ocean margin acts both as a net sink for the ^{230}Th produced in the inner ocean (boundary scavenging) but also as a net source of ^{232}Th for the open ocean. This illustrates the concept of boundary exchange developed with Nd isotopes where ocean margins play simultaneously the role of source and sink for a chemical element (Lacan and Jeandel, 2005).

The effect of the dissolution of the lithogenic inputs to the N. Pacific on the Nd isotopic composition of the Pacific deep water can be evaluated. Assuming that the lithogenic Nd is dissolved at the same extent as ^{232}Th (1%), a total flux of Nd $F_{\mathrm{Nd-litho}}$=1.9×10^9 g/y is released in the North Pacific margin. The average Nd isotopic composition is $\varepsilon_{\mathrm{Nd-litho}}\approx+6\pm4$ (Jeandel et al., 2007). This Nd is mixed with the Nd carried from the south Pacific by the thermohaline circulation. Using a water flow of 36×10^6 m^3/s (Table 1) and an average dissolved Nd concentration of 4 ng/l in seawater, we obtain an input of $F_{\mathrm{Nd-southPacific}}$=$3.8\times10^9$ g/y with an average Nd isotopic composition $\varepsilon_{\mathrm{Nd-southPacific}}\approx-8$ (Jeandel et al., 2007). The Nd isotopic composition of the Pacific deep water is given by

$$\varepsilon_{\mathrm{Nd-northPac}}=\frac{F_{\mathrm{Nd-litho}}\times\varepsilon_{\mathrm{Nd-litho}}+F_{\mathrm{Nd-South\,Pac}}\times\varepsilon_{\mathrm{Nd-South\,Pac}}}{F_{\mathrm{Nd-litho}}+F_{\mathrm{Nd-South\,Pac}}} \quad (11)$$

I obtain $\varepsilon_{\mathrm{Nd-northPac}}\approx-3.7\pm1.2$, in very gross agreement with the average value of the North Pacific ($\varepsilon_{\mathrm{Nd}}\approx-4.5$ (Arsouze et al., 2007)). It suggests that dissolution of lithogenic particles at the ocean margin provides a suitable source of Nd to explain the change of Nd isotopic composition as already proposed by (Lacan and Jeandel, 2005). Hence, simultaneous measurement of Nd and Th profiles could improve the understanding of the boundary exchange process by coupling a source tracer (Nd) with a chronometer (Th). Using Nd and Th as analogs for the insoluble elements such as iron will provide strong constraints on the inputs of micronutrients in the ocean.

3.2 Arctic Ocean

3.2.1 ^{230}Th

The first ^{230}Th data in the Arctic Ocean revealed unusually high ^{230}Th concentrations that were explained by the very low particle flux in this area covered by sea-ice (Bacon et al., 1989). Subsequent works demonstrated that lower concentrations occurred, in particular close to the shelf zones (Cochran et al., 1995; Edmonds et al., 1998, 2004; Scholten

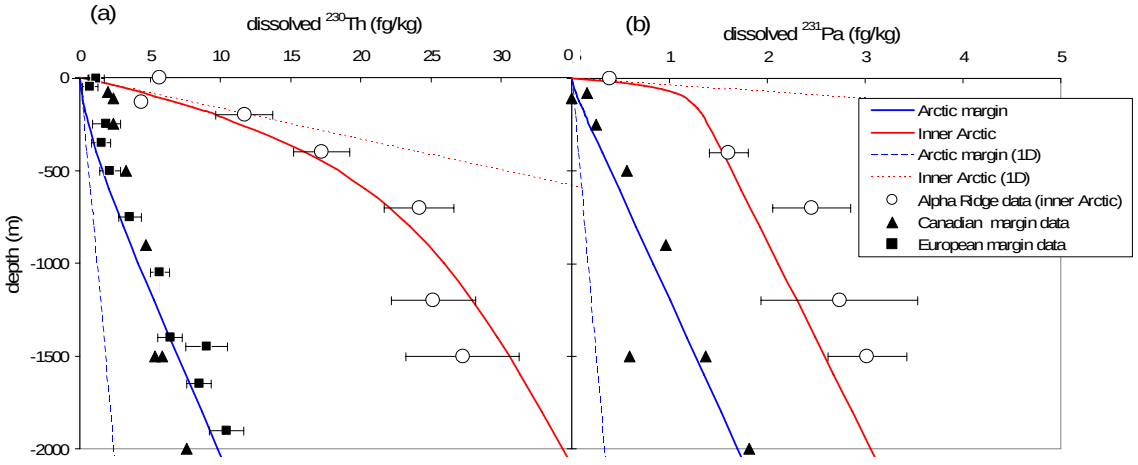


Fig. 3. Modelled profiles and comparison with data for the Arctic Ocean. See Table 1 for model parameters. "1-D" curves are obtained for the Arctic margin and inner Arctic Ocean by setting F=0 and keeping all the other parameters identical.

et al., 1995). The reversible scavenging model and the advection mixing model have generally failed to represent the low ^{230}Th concentrations in deep waters when using reasonable ventilation rates (Scholten et al., 1995). The ventilation rate on the Arctic Ocean is slow (Schlosser et al., 1995; Tanhua et al., 2009). In the Nansen Basin, the ventilation ages are of the order of a few years to decades for surface and halocline waters, 100 y for intermediate waters (500–1500 m), 200 y for deep water (1500–2500 m) and 300 y for bottom waters (>2500 m) (Schlosser et al., 1995). In the Canadian basin the ventilation of the intermediate, deep and bottom water is even slower, with a ventilation age of 450 y below 2000 m (Anderson et al., 1999; Schlosser et al., 1997). Over the Alpha ridge, the 200 m Atlantic water has CFC and ^{137}Cs ages of at least 30 y (Wallace and Moore, 1985). Deeper waters have very low anthropogenic tracer levels indicating long ventilation ages. It follows that the water ventilation is always slow compared to particulate transport. In the following discussion, I will neglect ventilation and just focus on the role of particle scavenging and horizontal advection on ^{230}Th transport.

During the 1990s, the Arctic Ocean has experienced significant changes. An increase of the warm Atlantic inflow was recorded in the Nansen, Amundsen and Makarov Basins. The Canadian basin remains relatively less affected. As the model assumes a steady state circulation, I compare the model with data collected during the 1980s or early 1990s in the European Basin and data collected during the 1990s and later for the Canada Basin. The inner ocean is represented by the CESAR station (85°50′ N, 108°50′ W) over the permanently ice-covered Alpha ridge (Bacon et al., 1989). I take as reference for the margin ocean, stations 287 (81°40′ N, 30°48′ E) and 423 (81°19.9′ N, 15°18.9′ E) sampled along the slope of the Nansen basin (Cochran et al., 1995)) in agreement with circulations schemes between the Alpha Ridge and the Nansen Basin (Rudels et al., 1994). As ^{231}Pa was not measured at these stations, I also use a station (72°32.59 N, 143°49.89 W) from the Canada basin with similar ^{230}Th concentration (Edmonds et al., 1998).

I consider waters above 2000 m because at greater depth the situation is complicated by the presence of oceanic ridges. The margin-inner ocean limit is set at the 2000 m isobath. The volume of the ocean margin (including marginal seas) is 1.55×10^6 km^3 and the central Arctic Ocean above 2000 m is 6.5×10^6 km^3. Surprisingly the margin/open ocean ratio is lower for the Arctic (1:4) than for the Pacific Ocean (1:3). This is because the shelves cover about 53% of the Arctic Ocean area, but contain only about 5% of the total Arctic Ocean volume (Jakobsson, 2002).

The transport is assumed to occur by eddy diffusion along isopycnal surfaces. An eddy diffusion coefficient of K_H=1.5×10^7 cm^2/s (Carmack et al., 1997) and a distance of 1500 km between the CESAR Station and the European shelf combined in Eq. (9) produce a mixing time $\Delta t\approx$40 y. It represents the time required for the water of the ocean margin to reach the inner ocean. Therefore, we set water residence time: τ_i=40 y, τ_m=10 y.

Knowing the concentration profiles, K_i and K_m from field data, the settling speeds are adjusted to obtain the best fit of the data (Table 1, Fig. 3a). Just like for ^{231}Pa in the Pacific, the "margin" and "inner ocean" ^{230}Th profiles become parallel at great depth. Below 500 m, the concentration difference between the 2 profiles at a given depth is equal to 20 fg/l. This difference is due to ^{230}Th ingrowth while water flows from the margin to the basin centre. Dividing this concentration difference by the production rate of ^{230}Th (0.54 fg/l/y) yields a time difference of 40 y. This is equal to the residence time of the water in the inner ocean because the scavenging rate is very low in the inner ocean and the water residence time is too short for the deep ^{230}Th concentration to reach

the linear equilibrium established in the shallow waters (Appendix B, Eq. B13).

The boundary scavenging profile model proposed here is the first model that accounts for the non-linear shape of the CESAR station ^{230}Th profile (remembering that the deep water ventilation is too slow to account for the shape of the profile). Similarly, margin-inner ocean interactions can explain why ^{230}Th concentrations lower than predicted with the 1-D model or the advection mixing model (using reasonable ventilation time) are found in the deep water of the Nansen, Amundsen and Makarov basins (Scholten et al., 1995).

Another important result of the model comes from the calculation of the ^{230}Th particulate flux to the sediment. At 2000 m, the ^{230}Th particulate flux ($S \times C_p$) represents 409% of the in situ production in the overlying water column at the margin and only 29 % in the inner ocean. This clearly shows that ^{230}Th may be strongly affected by boundary scavenging. An obvious consequence of this particle flux effect is that the particle settling velocity at the margin cannot be evaluated correctly with the 1-D model although the ^{230}Th profile increases linearly with depth. Using the 1-D model, the settling speed of the particles at the Nansen basin margin is 300 m/y whereas it is 600 m/y in the open Nansen basin, where one would expect a lower settling velocity (Cochran et al., 1995). In fact, one would expect a higher settling velocity rate of the particulate matter at the margin where the concentration of biological and lithogenic particles is the highest (and as a consequence the dissolved ^{230}Th concentration the lowest). The proposed explanation was that sediment resuspension could account for the lower calculated settling velocity at the margin. In fact, with the 1-D model, the settling velocity just depends on the particulate ^{230}Th concentration:

$$S = (P \times d)/^{230}\mathrm{Th}_p \quad (12)$$

where d is the water column height, so that, at a given depth, a high particulate ^{230}Th concentration always gives a low velocity.

With the boundary scavenging profile model, I estimate that the particle settling velocity is of the order of 1000 m/y. This value is much larger than the value (300 m/y based on the 6 y particulate Th residence time over a 2000 m water column calculated by (Cochran et al., 1995)) estimated with the 1-D-model because the sinking particulate matter must scavenge both the in situ production and the net input transported from the open ocean. This lateral transport is not represented in the 1-D model but it was already considered with the boundary scavenging box model of the Pacific Ocean (Anderson et al., 1983). The added value of the boundary scavenging profile model is to stress that a linear ^{230}Th profile (such as the profiles measured on the Arctic Ocean margins) does not guarantee that lateral transport can be neglected, as already shown by the study of thorium isotopes on and around the Kerguelen plateau (Venchiarutti et al., 2008).

As a consequence, a strong contrast in the accumulation rate of sedimentary ^{230}Th should exist between the open Arctic Ocean and its margins. Early evaluations of the ^{230}Th in arctic sediments suggested a strong ^{230}Th deficiency in the arctic sediments (Huh et al., 1997). A recent re-evaluation of the core ages has reduced this deficiency (Hoffmann and McManus, 2007) and demonstrated that high ^{230}Th accumulation rates ($\sim$2 times the local production rate) occur in the vicinity of the Chukchi shelf during the Holocene. ^{230}Th accumulation rates equivalent to the overlying production rate are observed towards the open ocean. Cores from the areas of the lowest sediment accumulation rates have not been measured in (Hoffmann and McManus, 2007).

3.2.2 ^{231} Pa

In order to obtain modelled profiles consistent with the available data (Fig. 3b), I use the settling speed obtained with ^{230}Th in the previous section, $K_i^{Pa} \approx K_i^{Th}/10$ in the inner Arctic Ocean (similar to the inner the Pacific ocean) and $K_m^{Pa} \approx K_m^{Th}/3$ for the Arctic margin (slightly larger ^{231}Pa/^{230}Th fractionation than in the Pacific margin) in agreement with the available data (Moran et al., 2005; Scholten et al., 1995). As already noted for ^{230}Th, a linear ^{231}Pa profile at the margin does not demonstrate that ^{231}Pa transport is dominated by vertical transport by particles rather than by lateral transport as proposed by (Edmonds et al., 1998).

A salient feature of the ^{231}Pa-^{230}Th fractionation in arctic sediments is that almost all ^{231}Pa/^{230}Th ratios in top-core sediments are lower than or equal to the production ratio of these nuclides in seawater even in ocean margin sites (Moran et al., 2005; Scholten et al., 1995). It was proposed that 40% of the Pa produced in the Arctic Ocean is exported in the Norwegian and Greenland seas through the Fram Straight, but sediments of the and Greenland sea do not show the high ^{231}Pa/^{230}Th ratios that would be expected in case of arrival of Pa from the Arctic Ocean. The boundary scavenging profile model suggests another process that could contribute to the lack of high ^{231}Pa/^{230}Th ratio in the sediments of the Arctic margins. The modelled ^{231}Pa/^{230}Th ratio in the particles of the open Arctic Ocean at 2000 m (and thus the ratio expected in the open ocean sediments) is below the production ratio, but the ^{231}Pa/^{230}Th ratio in the particles of the Arctic margin at 2000 m are only slightly higher than the production ratio (Table 1). This is because the scavenging rate of ^{231}Pa and ^{230}Th is so low in the open Arctic Ocean that most nuclides are scavenged at the ocean margin so that little ^{231}Pa/^{230}Th fractionation occurs compared to the production ratio. The difference with other oceans is that in the Arctic there could be a substantial lateral transport of ^{230}Th from the open ocean to the margins.

3.2.3 Comparison with other models

Following the seminal work of the 1-D scavenging model, various models have been proposed to describe the impact of

lateral transport on ^{230}Th and ^{231}Pa profiles. In the South Atlantic, the strong upwelling of the deep water masses cannot be neglected so that the ^{230}Th and ^{231}Pa profiles in this area were modelled by considering the transport of the nuclides by a reversible scavenging and the homogeneous advection of a water mass with a constant concentration throughout the water column (Rutgers van der Loeff and Berger, 1993). This model is now currently used to model ^{230}Th and ^{231}Pa profiles when upwelling or ventilation are important (Coppola et al., 2006; Moran et al., 2002; Roy-Barman et al., 2002). In particular, this model accounts for the low Pa and Th concentrations found in the deep waters of the Atlantic due to the presence of recently ventilated waters that have lost their Th and Pa by scavenging when they were at the surface (Scholten et al., 2008). It must be noted that boundary scavenging can produce Th and Pa profiles with low concentrations in the deep waters, a feature only modelled in the case of deep water ventilation until now. As a consequence, further work will have to consider the combined role of ventilation and boundary scavenging on Th and Pa profiles in the deep waters and the possible impact of boundary scavenging on the estimate of the ventilation rate based on Pa and Th data.

Recently, the effect of lateral transport was taken into account in a simple modelling of thorium isotopes in order to evaluate the settling speed of marine particles on the Kerguelen plateau that is a place or high biological productivity (due to an iron-induced bloom) surrounded by the HNLC Southern Ocean. In this model, open ocean water with a ^{230}Th concentration increasing linearly with depth is advected on the plateau. Advection and reversible scavenging on the plateau were used to explain the ^{230}Th concentration profile on the plateau (Venchiarutti et al., 2008). The Kerguelen plateau model is a particular case of the boundary scavenging profile model. In the case of the Kerguelen plateau, the ^{230}Th content of the open ocean water is considered as a fixed parameter and the scavenging conditions on the plateau have no feedback on this profile, because it seems reasonable to consider that the ^{230}Th content of the open Southern Ocean is not significantly influenced by the enhanced scavenging on the small Kerguelen plateau. On the contrary in the boundary scavenging profile model, the open ocean concentration is not fixed but it may be affected by the scavenging on the margins. Mathematically, the Kerguelen plateau model is equivalent to the boundary scavenging profile model with infinitely large open ocean volume (Appendix B, Sect. B4.). Contrary to the Kerguelen plateau model described above, the boundary scavenging profile model takes into account advection and scavenging to evaluate the ^{230}Th profiles simultaneously in the inner ocean and at the margin.

Regional and global circulation models coupled with biogeochemical models of various complexities are used to study the impact of circulation on the distribution of ^{230}Th and ^{231}Pa in the ocean as well as the possible constraints brought by ^{230}Th and ^{231}Pa on the thermohaline circulation (Dutay et al., 2009; Henderson et al., 1999, Siddall et al., 2005, 2007, 2008). These models successfully represent the preferential accumulation of particle reactive nuclides in the sediments of ocean margins but they have not been used directly to evaluate the impact of boundary scavenging on ^{230}Th and ^{231}Pa distribution in the water column. It must be noted that due to the paucity of data, these models are often underconstrained to discuss ^{230}Th or ^{231}Pa in a given region. Recently, (Marchal et al., 2007) used a constant and homogeneous particle flux over the whole Atlantic Ocean in order to use ^{230}Th as tracer of the thermohaline circulation. With regard to these sophisticated models, the present work underlines that the particle effect found at the ocean margin is not only due to a higher concentration of particulate matter but also to a faster settling rate of these particles, probably through aggregation/disagregation with the large settling particles. It stresses that more complex particle dynamics has to be used for these coupled physical-biogeochemical models as proposed by (Dutay et al., 2009). This would be particularly important for example to take into account geographical and/or temporal evolution of the ballasting effect.

4 Conclusions

The aim of the boundary scavenging profile model is not to describe precisely the Th and Pa profiles of any complicated "real" situation. It is rather to provide a simple theoretical framework where some effects of lateral transport on Th and Pa profiles can be evaluated and tested against observations. One of its important outputs is that a "more or less" linear ^{230}Th profile does not necessarily imply that advection is negligible as assumed in the 1D model and implies a re-evaluation of the ^{230}Th-based mean settling speed of particulate matter particularly in the coastal area. With the availability of high precision data measured by Thermal Ionisation Mass Spectrometry or by Induced Coupled Plasma Mass Spectrometry, it becomes obvious that the non-linear ^{230}Th profiles are more the rule than the exception even though linear profiles do exist (Roy-Barman et al., 1996). Until now, these non-linear profiles were generally attributed to upwelling or water mass ventilation. The model proposed in the present article allows a quantitative assessment of the effect of boundary scavenging which was suspected to produce non-linear profiles too. More generally, it allows a first order quantification of the effect of oceanic circulation on Pa and Th distribution in the water columns of areas with distinct scavenging conditions (margin/open ocean, subtropical gyre/equatorial area (Broecker, 2008), subtropical gyre/subpolar gyre (Taguchi et al., 1989)). This model should be useful for the numerous Pa-Th studies launched in the framework of the GEOTRACES program.

Appendix A

Resolution of the equations

A1 General solution

In the boundary scavenging profile model, the margin and the ocean interior works symmetrically (they only differ by the value of the constants S and K), so that Eq. (3a) and (3b) are symmetrical with respect to the margin and the open ocean. Therefore, it is sufficient to solve these equations for C_d^i to be able to deduce C_d^m by symmetry. These 2 equations are coupled by the lateral transport term. Using Eq. (3b), C_d^m can be expressed as a function of the other variables:

$$C_d^m = \frac{S_i V_i K_i}{F(1+K_m)} \frac{dC_d^i}{dz} - \frac{P V_i}{F(1+K_m)} + \frac{(1+K_i)}{(1+K_m)} C_d^i \quad \text{(A1)}$$

Derivating A1, gives the expression:

$$\begin{aligned} \frac{dC_d^m}{dz} &= \frac{d\left(\frac{S_i V_i K_i}{F(1+K_m)} \frac{dC_d^i}{dz} - \frac{P V_i}{F(1+K_m)} + \frac{(1+K_i)}{(1+K_m)} C_d^i\right)}{dz} \\ &= \frac{S_i V_i K_i}{F(1+K_m)} \frac{d^2 C_d^i}{dz^2} + \frac{(1+K_i)}{(1+K_m)} \frac{dC_d^i}{dz} \end{aligned} \quad \text{(A2)}$$

Combining Eqs. (A2) and (3a), we obtain:

$$\begin{aligned} &-S_m K_m \left(\frac{S_i V_i K_i}{F(1+K_m)} \frac{d^2 C_d^i}{dz^2} + \frac{(1+K_i)}{(1+K_m)} \frac{dC_d^i}{dz} \right) + P \\ &+\frac{F}{V_m}\left[(1+K_i) C_d^i - (1+K_m)\left(\frac{S_i V_i K_i}{F(1+K_m)} \frac{dC_d^i}{dz} - \frac{P V_i}{F(1+K_m)} + \frac{(1+K_i)}{(1+K_m)} C_d^i \right) \right] \\ &= 0 \end{aligned} \quad \text{(A3)}$$

which simplifies into:

$$\begin{aligned} &-\frac{S_i S_m K_i K_m V_i}{F(1+K_m)} \frac{d^2 C_d^i}{dz^2} \\ &-\left[S_m K_m \frac{(1+K_i)}{(1+K_m)} + \frac{S_i V_i K_i}{V_m} \right] \frac{dC_d^i}{dz} + P\left(1+\frac{V_i}{V_m}\right) = 0 \end{aligned} \quad \text{(A4)}$$

Equation (A4) can be written as:

$$a \frac{d^2 C_d^i}{dz^2} + b \frac{dC_d^i}{dz} + c = 0 \quad \text{(A5)}$$

with

$$a = -\frac{S_i S_m K_i K_m V_i}{F(1+K_m)} \quad \text{(A6a)}$$

$$b = -\left[S_m K_m \frac{(1+K_i)}{(1+K_m)} + \frac{S_i V_i K_i}{V_m} \right] \quad \text{(A6b)}$$

$$c = P\left(1+\frac{V_i}{V_m}\right) \quad \text{(A6c)}$$

Integrating this equation a first time, we obtain:

$$a \frac{dC_d^i}{dz} + b C_d^i = -cz + d_1 \quad \text{(A7)}$$

where d_1 is an integration constant. The solution of Eq. (A5) can be written:

$$C_d^i = f e^{-(\frac{b}{a})z} \quad \text{(A8)}$$

here f is a function of z. Substituting this expression in Eq. (A7), we obtain:

$$a \frac{df}{dz} e^{-(\frac{b}{a}z)} = -cz + d_1 \quad \text{(A9)}$$

so that:

$$\frac{df}{dz} = -\frac{cz+d_1}{a} e^{(\frac{b}{a})z} \quad \text{(A10)}$$

The primitive of this function can be written as

$$f = (\frac{-c}{b} z + \frac{ac+d_1 b}{b^2}) e^{(\frac{b}{a})z} + d_2 \quad \text{(A11)}$$

where d_2 is an integration constant. Substituting Eq. (A11) in Eq. (A8), we obtain:

$$C_d^i = -\frac{c}{b} z + \frac{ac+d_1 b}{b^2} + d_2 e^{-(\frac{b}{a})z} \quad \text{(A12)}$$

It is now necessary to determine the value of d_1 and d_2 with 2 boundary conditions. At z=0, the vertical particulate flux ($C_p \times$S) must be equal to the atmospheric input (Φ). It follows that

$$C_p^m(z=0) = \frac{\Phi_m}{S_m} \quad \text{(A13a)}$$

$$C_p^i(z=0) = \frac{\Phi_i}{S_i} \quad \text{(A13b)}$$

and because $C_p = K C_d$ (Eq. 2):

$$C_d^m(z=0) = \frac{\Phi_m}{K_m S_m} \quad \text{(A13c)}$$

$$C_d^i(z=0) = \frac{\Phi_i}{K_i S_i} \quad \text{(A13d)}$$

For the inner ocean, combining Eq. (A12) and Eq. (A13d) for z=0 gives:

$$C_d^i(z=0) = +\frac{ac+d_1 b}{b^2} + d_2 = \frac{\Phi_i}{K_i S_i} \quad \text{(A14)}$$

For the margin, combining Eq. (A1) and Eq. (A12), gives

$$\begin{aligned} C_d^m = &\frac{S_i V_i K_i}{F(1+K_m)} \frac{d\left(-\frac{c}{b}z + \frac{ac+d_1 b}{b^2} + d_2 e^{-(\frac{b}{a})z}\right)}{dz} - \frac{P V_i}{F(1+K_m)} \\ &+ \frac{(1+K_i)}{(1+K_m)} \left(-\frac{c}{b}z + \frac{ac+d_1 b}{b^2} + d_2 e^{-(\frac{b}{a})z}\right) \end{aligned} \quad \text{(A15)}$$

Calculating the derivative terms yield

$$\begin{aligned} C_d^m = &\frac{S_i V_i K_i}{F(1+K_m)} \left(-\frac{c}{b} - (\frac{b}{a}) d_2 e^{-(\frac{b}{a})z}\right) - \frac{P V_i}{F(1+K_m)} \\ &+ \frac{(1+K_i)}{(1+K_m)} \left(-\frac{c}{b}z + \frac{ac+d_1 b}{b^2} + d_2 e^{-(\frac{b}{a})z}\right) \end{aligned} \quad \text{(A16)}$$

at z=0, combining Eq. (A16) and Eq. (A13c), yields:

$$\begin{aligned} C_d^m(z=0) = & \frac{S_i V_i K_i}{F(1+K_m)}\left(-\frac{c}{b}-(\frac{b}{a})d_2\right) \\ & -\frac{PV_i}{F(1+K_m)}+\frac{(1+K_i)}{(1+K_m)}\left(\frac{ac+d_1 b}{b^2}+d_2\right) \\ & = \frac{\Phi_m}{K_m S_m} \end{aligned} \quad \text{(A17)}$$

Introducing Eq. (A14) in Eq. (A17), allows eliminating d_1:

$$\begin{aligned} & \frac{S_i V_i K_i}{F(1+K_m)}\left(-\frac{c}{b}-(\frac{b}{a})d_2\right)-\frac{PV_i}{F(1+K_m)} \\ & +\frac{(1+K_i)}{(1+K_m)}\left(\frac{\Phi_i}{K_i S_i}\right)=\frac{\Phi_m}{K_m S_m} \end{aligned} \quad \text{(A18)}$$

Equation (A18) allows determining d_2:

$$d_2 = -\left\{\frac{P}{S_i K_i}+\frac{c}{b}+\left(\frac{(1+K_m)\Phi_m}{K_m S_m}-\frac{(1+K_i)\Phi_i}{K_i S_i}\right)\frac{F}{S_i V_i K_i}\right\}(\frac{a}{b}) \quad \text{(A19)}$$

Combining Eq. (A12) with Eq. (A13d) at z=0, gives:

$$C_d^i(z=0)=\frac{ac+d_1 b}{b^2}+d_2=\frac{\Phi_i}{K_i S_i} \quad \text{(A20a)}$$

so that

$$\begin{aligned} C_d^i &= -\frac{c}{b}z+\left(\frac{\Phi_i}{K_i S_i}-d_2\right)+d_2 e^{-(\frac{b}{a})z} \\ &= -\frac{c}{b}z+d_2\left(e^{-(\frac{b}{a})z}-1\right)-\frac{\Phi_i}{K_i S_i} \end{aligned} \quad \text{(A20b)}$$

We note that

$$\begin{aligned} \frac{b}{a} &= \frac{\left[S_m K_m \frac{(1+K_i)}{(1+K_m)}+\frac{S_i V_i K_i}{V_m}\right]}{\frac{S_i S_m K_i K_m V_i}{F(1+K_m)}} \\ &= \frac{F}{V_i}\frac{(1+K_i)}{S_i K_i}+\frac{F}{V_m}\frac{(1+K_m)}{S_m K_m} \end{aligned} \quad \text{(A21)}$$

So z_0 is defined as:

$$z_0=\left(\frac{F}{V_i}\frac{(1+K_i)}{S_i K_i}+\frac{F}{V_m}\frac{(1+K_m)}{S_m K_m}\right)^{-1} \quad \text{(A22)}$$

$1/z_0$ is the e-folding term of the vertical evolution of the slope of the concentrations ($\mathrm{d}C/\mathrm{d}z$) and of the concentrations themselves (Eqs. A5 and A7). z_0 represents a depth below which lateral mixing becomes significant compared to particulate transport.

$$\begin{aligned} \frac{c}{b} &= -\frac{\left(P+P\frac{V_i}{V_m}\right)}{S_m K_m \frac{(1+K_i)}{(1+K_m)}+\frac{S_i V_i K_i}{V_m}} \\ &= -\frac{1}{(1+K_i)}\frac{P(V_m+V_i)}{\frac{S_m K_m V_m}{(1+K_m)}+\frac{S_i V_i K_i}{(1+K_i)}} \end{aligned} \quad \text{(A23)}$$

We note:

$$\sigma_\infty = \frac{P(V_m+V_i)}{\frac{S_m K_m V_m}{(1+K_m)}+\frac{S_i V_i K_i}{(1+K_i)}} \quad \text{(A24)}$$

σ_∞ represents the slope of the dissolved + particulate ^{230}Th concentration versus depth profiles at great depth for the margin and the inner ocean.

Introducing Eq. (A19) and (A21)–(A24) in Eq. A20b gives the final expression of C_d^i:

$$\begin{aligned} C_d^i &= \frac{\sigma_\infty}{(1+K_i)}\times z+\frac{\Phi_i}{K_i S_i} \\ &+\left(\frac{P}{S_i K_i}-\frac{\sigma_\infty}{(1+K_i)}+\left(\frac{(1+K_m)\Phi_m}{K_m S_m}-\frac{(1+K_i)\Phi_i}{K_i S_i}\right)\frac{F}{S_i V_i K_i}\right) \\ &\times z_0\times\left(1-e^{-\left(\frac{z}{z_0}\right)}\right) \end{aligned} \quad \text{(A25a)}$$

The term $\frac{1}{(1+K_i)}$ converts total ^{230}Th into dissolved ^{230}Th in the ocean interior. Notting that the problem is mathematically symmetrical with regard to the ocean margin and the inner ocean, the concentration in the coastal ocean is given by:

$$\begin{aligned} C_d^m &= \frac{\sigma_\infty}{(1+K_m)}\times z+\frac{\Phi_m}{K_m S_m} \\ &+\left(\frac{P}{S_m K_m}-\frac{\sigma_\infty}{(1+K_m)}+\left(\frac{(1+K_i)\Phi_i}{K_i S_i}-\frac{(1+K_m)\Phi_m}{K_m S_m}\right)\frac{F}{S_m V_m K_m}\right) \\ &\times z_0\times\left(1-e^{-\left(\frac{z}{z_0}\right)}\right) \end{aligned} \quad \text{(A25b)}$$

A2 Solution for in situ produced nuclide (^{230}Th$_{xs}$ and ^{231}Pa$_{xs}$)

For ^{230}Th and ^{231}Pa, we are interested by their in situ produced fraction represented by ^{230}Th$_{xs}$ and ^{231}Pa$_{xs}$. Therefore, the atmospheric inputs are taken equal to zero (Φ_i=Φ_m=0). With these conditions the profiles are given by:

$$\begin{aligned} C_d^i &= \frac{\sigma_\infty}{(1+K_i)}\times z+\left(\frac{P}{S_i K_i}-\frac{\sigma_\infty}{(1+K_i)}\right) \\ &\times z_0\times\left(1-e^{-\left(\frac{z}{z_0}\right)}\right) \end{aligned} \quad \text{(A26a)}$$

$$\begin{aligned} C_d^m &= \frac{\sigma_\infty}{(1+K_m)}\times z+\left(\frac{P}{S_m K_m}-\frac{\sigma_\infty}{(1+K_m)}\right) \\ &\times z_0\times\left(1-e^{-\left(\frac{z}{z_0}\right)}\right) \end{aligned} \quad \text{(A26b)}$$

A3 Solution for external inputs only (^{232}Th)

Dissolved ^{232}Th is produced by dissolution of lithogenic material. There is no in situ production (P=0) so that σ_∞=0. It is assumed that all ^{232}Th dissolution (eolian and riverine sources) occurs in the surface waters, so that $\Phi_i \neq 0$ and $\Phi_m \neq 0$. With these conditions the profiles are given by:

$$\begin{aligned} C_d^i &= \left(\frac{(1+K_m)\Phi_m}{K_m S_m}-\frac{(1+K_i)\Phi_i}{K_i S_i}\right)\frac{F}{S_i V_i K_i} \\ &\times z_0\times\left(1-e^{-\left(\frac{z}{z_0}\right)}\right)+\frac{\Phi_i}{K_i S_i} \end{aligned} \quad \text{(A27a)}$$

$$\begin{aligned} C_d^m &= \left(\frac{(1+K_i)\Phi_i}{K_i S_i}-\frac{(1+K_m)\Phi_m}{K_m S_m}\right)\frac{F}{S_m V_m K_m} \\ &\times z_0\times\left(1-e^{-\left(\frac{z}{z_0}\right)}\right)+\frac{\Phi_m}{K_m S_m} \end{aligned} \quad \text{(A27b)}$$

Appendix B

Particular cases for in situ produced nuclides

B1 Identical scavenging conditions for the margin and the ocean interior

When $K_m{=}K_i{=}K$ and $S_m = S_i = S$, Eqs. (A23) and (A24) become:

$$\frac{c}{b} = \frac{P}{SK} \tag{B1}$$

$$\sigma_\infty = (1+K)\frac{P}{SK} \tag{B2}$$

So that Eq. (26a) and (26b) become:

$$C_d^i = C_d^m = \frac{P}{SK} \times z = \frac{\sigma_\infty}{1+K} \times z \tag{B3}$$

If the scavenging conditions are identical for the margin and the ocean interior, the net effect of advection can be neglected and ^{230}Th has a linear profile over the whole basin.

B2 Close to the surface or if the residence time of the water is very long

Close to the surface or if the residence time of the water is very long: $z/z_0 \ll 1$

Then

$$e^{-(z/z_0)} \approx 1 - \frac{z}{z_0} \tag{B4}$$

Substituting Eq. (B4) in (A26a)

$$C_d^i \approx \frac{\sigma_\infty}{(1+K_i)} \times z + \left(\frac{P}{S_i K_i} - \frac{\sigma_\infty}{(1+K_i)}\right) \times z_0 \times \left(\frac{z}{z_0}\right) \tag{B5}$$

So that

$$C_d^i \approx \frac{P}{S_i K_i} \times z \tag{B6a}$$

and similarly for Eq. (B4) in (A26b)

$$C_d^m \approx \frac{P}{S_m K_m} \times z \tag{B6b}$$

Close to the surface ($z \to 0$) or if the residence time of the water is very long in both margin *and* the open ocean ($z_0 \to +\infty$), the effect of lateral transport is negligible and the profiles are identical to those obtained without advection. At the sea surface (z=0), $C_d^i{=}C_m^i{=}0$, so that there is no horizontal concentration gradient and the effect of lateral transport is null. In contrast, at the sea surface, the vertical concentration gradient is not equal to zero so that the vertical transport entirely balances the in situ production.

As a consequence, it may be safe to determine the settling speed of marine particles with ^{230}Th data collected in the upper part of the water column rather than with the deep water data that are more affected by boundary scavenging.

B3 At great depth or with a short water residence time in one of the reservoir

When $z \to +\infty$ (great depth) or $z_0 \to 0$ (short water residence time in at least one of the reservoir), then $z \gg z_0$

In this case:

$$e^{-\left(\frac{z}{z_0}\right)} \approx 0 \tag{B7}$$

Introducing Eq. (B7) in (A26a) and (A26b) yields:

$$C_t^i \approx \sigma_\infty \times z + \left((1+K_i)\frac{P}{S_i K_i} - \sigma_\infty\right) \times z_0 \tag{B8a}$$

$$C_t^m \approx \sigma_\infty \times z + \left((1+K_m)\frac{P}{S_m K_m} - \sigma_\infty\right) \times z_0 \tag{B8a}$$

These equations represent straight lines with identical slopes but and a constant concentration offset between them. The concentration difference at a given depth is:

$$C_t^i - C_t^m \approx \left((1+K_i)\frac{P}{S_i K_i} - (1+K_m)\frac{P}{S_m K_m}\right) \times z_0 \tag{B9}$$

So that:

$$\frac{C_t^i - C_t^m}{P} \approx \left(\frac{1+K_i}{S_i K_i} - \frac{1+K_m}{S_m K_m}\right) \times z_0 \tag{B10}$$

If the scavenging rate and the settling speed are much greater in the ocean margin ($S_m K_m \ll S_i K_i$), Eq. (B10) and (A21) become:

$$\frac{C_t^i - C_t^m}{P} \approx \frac{1+K_i}{S_i K_i} \times z_0 \tag{B11}$$

$$z_0 \approx \left(\frac{F}{V_i}\frac{(1+K_i)}{S_i K_i}\right)^{-1} \tag{B12}$$

So that

$$\frac{C_t^i - C_t^m}{P} \approx \frac{(1+K_i)}{S_i K_i} \times z_0 \approx \frac{V_i}{F} = \tau_i \tag{B13}$$

$\frac{C_t^i - C_t^m}{P}$ is the time required to generate this concentration difference by in situ radioactive production assuming that there is no scavenging, i.e., approximately the time spent by the water mass in the open ocean since it left the ocean margin (τ_i). In fact, it is lower than τ_i, because scavenging in the open ocean removes part of the nuclides produced during τ_i.

Ultimately, as z increases, the second term of the right hand-side of Eq. (B8a) and (B8b) becomes negligible, so that these equations become

$$C_t^i \approx \sigma_\infty \times z \tag{B14a}$$

and

$$C_t^m \approx \sigma_\infty \times z \tag{B14b}$$

It means that when the water residence time is small compared to scavenging time in one of the reservoir at least, the total ^{230}Th concentration is homogenized by lateral mixing.

Theoretically, the C_t^i and C_t^m are never perfectly equal at a given depth as indicated by Eq. (B10), but as depth increases the difference of concentration $C_t^i - C_t^m$ becomes small compared to the concentration themselves.

B4 Comparison of the boundary scavenging profile model with Venchiarutti et al. (2008)

If $V_i \gg V_m$ and $\frac{S_i V_i K_i}{(1+K_i)} \gg \frac{S_m K_m V_m}{(1+K_m)}$ (the inner ocean is much larger than the ocean margin and despite a lower scavenging rate in the inner ocean most of the ^{230}Th is scavenged in the inner ocean because its volume is so large compared to the margin).

Equation (A24) can be approximated by:

$$\sigma_\infty \approx (1+K_i)\frac{P}{S_i K_i} \tag{B15}$$

and Eq. (A22) can be approximated by:

$$z_0 \approx \frac{V_m}{F}\frac{S_m K_m}{(1+K_m)} \tag{B16}$$

So that Eq. (A26a) and (A26b) become:

$$C_d^i = \frac{P}{S_i K_i} \times z \tag{B17a}$$

(the profile increases linearly in the open ocean)

$$C_d^m = \frac{(1+K_i)}{(1+K_m)}\frac{P}{S_i K_i} \times z + \left(\frac{P}{S_m K_m} - \frac{(1+K_i)}{(1+K_m)}\frac{P}{S_i K_i}\right) \times z_0 \times \left(1 - e^{-\left(\frac{z}{z_0}\right)}\right) \tag{B17b}$$

Using Eq. (B14), Eq. (B16b) can be arranged as:

$$C_d^m = \left(\frac{P}{S_m K_m}\right) \times z_0 \times \left(1 - e^{-\left(\frac{z}{z_0}\right)}\right) + \left(\frac{\sigma_\infty}{(1+K_m)}\right) \times z_0 \times \left(\frac{z}{z_0} - 1 + e^{-\left(\frac{z}{z_0}\right)}\right) \tag{B18}$$

This expression is equivalent to Eq. (13) obtained in Venchiarutti et al. (2008).

Acknowledgements. The author thanks C. Jeandel for her encouragements to achieve this project. The comments of C. Jeandel, C. Venchiarutti and J.-C. Dutay significantly improved the manuscript. M. Siddall has provided interesting discussions concerning particle flux modelling. M. Rutgers van der Loeff and R. Anderson are acknowledged for their thorough reviews. This is LSCE contribution 4019.

Edited by: C. Heinze



The publication of this article is financed by CNRS-INSU.

References

Anderson, L. G., Jones, E. P., and Rudels, B.: Ventilation of the Arctic Ocean estimated by a plume entrainment model constrained by CFCs, J. Geophys. Res., 104, 13 423–13 429, 1999.

Anderson, R. F., Bacon, M. P., and Brewer, P. G.: Removal of ^{231}Pa and ^{230}Th at ocean margins, Earth Planet. Sc. Lett., 66, 73–90, 1983.

Arraes-Mescoff, R., Coppola, L., Roy-Barman, M., Souhaut, M., Tachikawa, K., Jeandel, C., Sempéré, R., and Yoro, C.: The behavior of Al, Mn, Ba, Sr, REE and Th isotopes during *in vitro* bacterial degradation of large marine particles, Mar. Chem., 73, 1–19, 2001.

Arsouze, T., Dutay, J.-C., Lacan, F., and Jeandel, C.: Modelling the neodymium isotopic composition with a global ocean general circulation model, Chem. Geol., 239, 165–177, 2007.

Bacon, M. P.: ^{210}Pb and ^{210}Po results from F. S. Meteor cruise 32 in the North Atlantic, Meteor. Forschungs-Ergebnisse, 19, 24–36, 1977.

Bacon, M. P.: Tracers of chemical scavenging in the ocean: boundary effects and large scale chemical fractionation, Philos. T. Roy. Soc. A, 325, 147–160, 1988.

Bacon, M. P. and Anderson, R. F.: Distribution of thorium isotopes between dissolved and particulate forms in the Deep-Sea, J. Geophys. Res., 87, 2045–2056, 1982.

Bacon, M. P., Huh, C.-A., and Moore, R. M.: Vertical profiles of some natural radionuclides over the Alpha Ridge, Arctic Ocean, Earth Planet. Sc. Lett., 95, 15–22, 1989.

Bacon, M. P., Huh, C.-H., Fleer, A. P., and Deuser, W. G.: Seasonality in the flux of natural radionuclides and plutonium in the deep Sargasso Sea, Deep-Sea Res., 32, 273–286, 1985.

Boyle, E. A., Berquist, B. A., Kayser, R. A., and Mahowald, N.: Iron, manganese, and lead at Hawaii Ocean Time-series station ALOHA: Temporal variability and an intermediate water hydrothermal plume, Geochim. Cosmochim. Ac., 69, 933–952, 2005.

Broecker, W.: Excess sediment ^{230}Th: Transport along the sea floo or enhanced water column scavenging?, Global Biogeochem. Cy., 22, GB1006, doi:10.1029/2007GB003057, 2008.

Carmack, E. C., Aagaard, K., Swift, J. H., Macdonald, R. W., McLaughlin, F. A., Jones, E. P., Perkin, R. G., Smith, J. N., Ellis, K. M., and Kilius, L.: Changes in temperature and tracer distributions within the Arctic Ocean: Results from the 1994 Arctic Ocean Section, Deep-Sea Res. Pt. II, 44, 1487–1502, 1997.

Chase, Z., Anderson, R. F., Fleisher, M. Q., and Kubik, P. W.: The influence of particle composition and particle flux on scavenging of Th, Pa and Be in the ocean, Earth Planet. Sc. Lett., 204, 215–229, 2002.

Cochran, J. K., Hirschberg, D. J., Livingston, H. D., Buesseler, K. O., and Key, R. M.: Natural and anthropogenic radionuclide distributions in the Nansen Basin, Arctic Ocean: scavenging rates and circulation timescales, Deep-Sea Res. Pt. II, 42, 1495–1517, 1995.

Coppola, L., Roy-Barman, M., Mulsow, S., Povinec, P., and Jeandel, C.: Thorium isotopes as tracers of particles dynamics and deep water circulation in the Indian sector of the Southern Ocean (ANTARES IV), Mar. Chem., 100, 299–313, 2006.

Duce, R. A., Liss, P. S., Merrill, J. T., Atlas, E. L., Buat-Ménard, P., Hicks, B. B., Miller, J. M., Prospero, J. M., Arimoto, R., Church, T. M., Ellis, W., Galloway, J. N., Hansen, L., Jickells, T. D., Knap, A. H., Reinhardt, K. H., Schneider, B., Soudine, A., Tokos, J. J., Tsunogai, S., Wollast, R., and Zhou, M.: The atmospheric input of trace species to the world ocean., Global Biogeochem. Cy., 5, 193–259, 1991.

Dutay, J.-C., Lacan, F., Roy-Barman, M., and Bopp, L.: Study of the influence of the particles' size and type on the simulation of ^{231}Pa and ^{230}Th with a global coupled biogeochemical- ocean general circulation model: a first approach, Geochem. Geophy. Geosy., 10, Q01011, doi:10.1029/2008GC002291, 2009.

Edmonds, H. N., Moran, S. B., Cheng, H., and Edwards, R. L.: ^{230}Th and ^{231}Pa in the Arctic Ocean: implications for particle fluxes and basin-scale Th/Pa fractionation, Earth Planet. Sc. Lett., 227, 155–167, 2004.

Edmonds, H. N., Moran, S. B., Hoff, J. A., Smith, J. N., and Edwards, R. L.: Protactinium-231 and Thorium-230 abundances and high scavenging rates in the Western Arctic Ocean, Science, 280, 405–407, 1998.

Fine R. A., Maillet K. A., Sullivan K. F., and Willey D.: Circulation and ventilation flux of the Pacific Ocean, J. Geophys. Res., 106, 22 159–22 178, 2001.

Henderson, G. M., Heinze, C., Anderson, R. F., and Winguth, A. M. E.: Global distribution of the ^{230}Th flux to ocean sediments constrained by GCM modelling, Deep-Sea Res. Pt. I, 46, 1861–1893, 1999.

Hoffmann, S. and McManus, J.: Is there a ^{230}Th deficit in Arctic sediments?, Earth Planet. Sc. Lett., 258, 516–527, 2007.

Huh, C.-A., Pisias, N. G., Kelley, J. M., Maiti, T. C., and Grantz, A.: Natural radionuclides and plutonium in sediments from the western Arctic Ocean: sedimentation rates and pathways of radionuclides, Deep-Sea Res. Pt. II, 44, 1725–1743, 1997.

Jakobsson, M.: Hypsometry and volume of the Arctic Ocean and its constituent seas, Geochem. Geophy. Geosy., 3, 1028, doi10.1029/2001GC000302, 2002.

Jeandel, C., Arsouze, T., Lacan, F., Téchiné, P., and Dutay, J.-C.: Isotopic Nd compositions and concentrations of the lithogenic inputs into the ocean: A compilation, with an emphasis on the margins, Chem. Geol., 239, 156–164, 2007.

Lacan, F. and Jeandel, C.: Neodymium isotopes as a new tool for quantifying exchange fluxes at the continent-ocean interface, Earth Planet. Sc. Lett., 232, 245–257, 2005.

Ledwell, J. R., Montgomery, E. T., Polzin, K. L., St Laurant, L. C., Schmitt, R. W., and Toole, J. M.: Evidence for enhanced mixing over rough topography in the abyssal ocean, Nature, 403, 179–82, 2000.

Ledwell, J. R., Watson, A. J., and Laws, C. S.: Mixing of a tracer in the pycnocline, J. Geophys. Res., 108, 21 499–21 529, 1998.

Marchal, O., François, R., and Scholten, I.: Contribution of ^{230}Th measurements to the estimation of the abyssal circulation, Deep-Sea Res. Pt. I, 54, 557–585, 2007.

Matsumoto, K.: Radiocarbon-based circulation age of the world oceans, J. Geophys. Res., 112, C09004, doi:10.1029/2007JC004095, 2007.

Milliman, J. D. and Meade, R. H.: World-wide delivery of river sediment to the oceans, J. Geol., 91, 1–21, 1983.

Moran, S. B., Shen, C.-C., Edmonds, H. N., Weinstein, S. E., Smith, J. N., and Edwards, R. L.: Dissolved and particulate ^{231}Pa and ^{230}Th in the Atlantic Ocean: constraints on intermediate/deep water age, boundary scavenging, and ^{231}Pa/^{230}Th fractionation, Earth Planet. Sc. Lett., 203, 999–1014, 2002.

Moran, S. B., Shen, C.-C., Edwards, R. L., Edmonds, H. N., Scholten, J. C., Smith, J. N., and Ku, T.-L.: ^{231}Pa and ^{230}Th in surface sediments of the Arctic Ocean: Implications for ^{231}Pa/^{230}Th fractionation, boundary scavenging and advective export, Earth Planet. Sc. Lett., 234, 235–248, 2005.

Munk, W.: Abyssal recipes, Deep-Sea Res., 13, 207–30, 1966.

Nozaki, Y., Horibe, Y., and Tsubota, H.: The water column distribution of thorium isotopes in the western North Pacific, Earth Planet. Sc. Lett., 54, 203–216, 1981.

Nozaki, Y. and Nakanishi, T.: ^{231}Pa and ^{230}Th in the open ocean water column, Deep-Sea Res., 32, 1209–1220, 1985.

Nozaki, Y., Yamada, M., Nakanishi, T., Nagaya, Y., Nakamura, K., Shitashima, K., and Tsbota, H.: The distribution of radionuclides and some trace metals in the water columns of the Japan and Bonin trenches, Oceanol. Acta, 21, 469–484, 1995.

Nozaki, Y., and Yang, H.-S.: Th and Pa isotopes in the waters of the western margin of the Pacific near Japan: Evidence for release of ^{228}Ra and ^{227}Ac from slope sediments, Journal of Oceanographic Society of Japan, 43, 217–227, 1987.

Nozaki, Y., Yang, H.-S., and Yamada, M.: Scavenging of thorium in the ocean, J. Geophys. Res., 92, 772–778, 1987.

Owens, W. B. and Warren, B. A.: Deep circulation in the northwest corner of the Pacific Ocean, Deep-Sea Res. Pt. I, 48, 959–993, 2001.

Reid, J. L.: On the total geostrophic circulation of the Pacific Ocean: flow patterns, tracers, and transports, Prog. Oceanogr., 39, 263–352, 1997.

Roy-Barman, M., Chen, J. H., and Wasserburg, G. J.: ^{230}Th-^{232}Th systematics in the Central Pacific Ocean: the sources and the fates of thorium, Earth Planet. Sc. Lett., 139, 351–363, 1996.

Roy-Barman, M., Coppola, L., and Souhaut, M.: Thorium isotopes in the Western Mediterranean Sea: an insight into the marine particle dynamics, Earth Planet. Sc. Lett., 196, 161–174, 2002.

Roy-Barman, M., Jeandel, C., Souhaut, M., Rutgers van der Loeff, M., Voege, I., Leblond, N., and Freydier, R.: The influence of particle composition on thorium scavenging in the NE Atlantic ocean (POMME experiment), Earth Planet. Sc. Lett., 240, 681–693, 2005.

Roy-Barman, M., Lemaître, C., Ayrault, S., Jeandel, C., Souhaut, M. and J.-C. Miquel: The influence of particle composition on Thorium scavenging in the Mediterranean Sea, Earth Planet. Sc. Lett., 286, 526–534, 2009.

Rudels, B., Jones, E. P., Anderson, L. G., and Kattner, G.: On the intermediate depth waters of the Arctic Ocean, in: The Polar Oceans and Their Role in Shaping the Global Environment, edited by: Johannessen, O. M., Muench, D., and Overland, J. E., Geophys. Monogr. Ser., AGU, Washington, D. C., 85, 33–46, 1994.

Rutgers van der Loeff, M. M. and Berger, G. W.: Scavenging of ^{230}Th and ^{231}Pa near the Antarctic Polar Front in the South Atlantic, Deep-Sea Res., 40, 339–357, 1993.

Santschi, P. H., Murray, J. W., Baskaran, M., Benitez-Nelson, C. R., Guo, L. D., Hung, C.-C., Lamborg, C., Moran, S. B., Passow, U., and Roy-Barman, M.: Thorium speciation in seawater, Mar. Chem., 100, 250–268, 2006.

Sarmiento, J. L. and Rooth, C. G. H.: A comparison of vertical and isopycnal mixing models in the deep sea based on radon 222 measurements, J. Geophys. Res., 85, 1515–1518, 1980.

Sarmiento, J. L., Rooth, C. G. H., and Broecker, W. S.: Radium 228 as a Tracer of Basin Wide Processes in the Abyssal Ocean, J. Geophys. Res., 87 , 9694–9698, 1982.

Schlosser, P., Bonisch, G., Kromer, B., Loosli, H. H., Bohler, B., Bayer, R., Bonani, G., and Kolterman, K. P.: Mid-1980s distribution of tritium, 3He, 14C and 39Ar in the Greenland/Norwegian Seas and the Nansen Basin of the Arctic Ocean, Prog. Oceanogr., 35, 1–28, 1995.

Schlosser, P., Kromer, B., Ekwurzel, B., Bönisch, G., McNichol, A., Schneider, R., von Reden, K., Ostlund, H. G., and Swift, J. H.: The first trans-Arctic 14C section: comparison of the mean ages of the deep waters in the Eurasian and Canadian basins of the Arctic Ocean, Nucl. Instrum. Meth. B, 123, 431–437, 1997.

Scholten, J. C., Fietzke, J., Mangini, A., Garbe-Schönberg, C.-D., Eisenhauer, A., Schneider, R., and Stoffers, P.: Advection and scavenging: Effects on ^{230}Th and ^{231}Pa distribution off Southwest Africa, Earth Planet. Sc. Lett., 271, 159–169, 2008.

Scholten, J. C., Rutgers van der Loeff, M. M., and Michel, A.: Distribution of ^{230}Th and ^{231}Pa in the water column in relation to the ventilation of the deep Arctic basins, Deep-Sea Res. Pt. II, 42, 1519–1531, 1995.

Siddall, M., Anderson, R. F., Winckler, G., Henderson, G. M., Bradtmiller, L. I., McGee, D., Franzese, A., Stocker, T. F., and Müller, S. A.: Modeling the particle flux effect on distribution of 230Th in the equatorial Pacific, Paleoceanography, 23, PA2208, doi:10.1029/2007PA001556, 2008.

Siddall, M., Henderson, G. M., Edwards, N. R., Müller, S. A., Stocker, T. F., Joos, F., and Frank, M.: 231Pa/230Th fractionation by ocean transport, biogenic particle flux and particle type, Earth Planet. Sc. Lett., 237, 137–155., 2005.

Siddall, M., Stocker, T. F., Henderson, G. M., Joos, F., Frank, M., Edwards, N. R., Ritz, S., and Müller, S. A.: Modelling the relationship between ^{231}Pa/^{230}Th distribution in North Atlantic sediment and Atlantic Meridional Overturning Circulation, Paleoceanography, 22, PA2214, doi:10.1029/2006PA001358, 2007.

Spencer, D. W., Bacon, M. P., and Brewer, P. G.: Models of the distribution of 210Pb in a section across the north Equatorial Atlantic Ocean, J. Mar. Res., 39, 119–138, 1981.

Taguchi, K., Harada, K., and Tsunogai, S.: Particulate removal of ^{230}Th and ^{231}Pa in the biologically productive northern North Pacific, Earth Planet. Sc. Lett., 93, 223–232, 1989.

Tanhua, T., Jones, E. P., Jeansson, E., Jutterström, S., Smethie, W. M., Wallace, D. W. R., and Anderson, L. G.: Ventilation of the Arctic Ocean: mean ages and inventories of anthropogenic CO_2 and CFC-11, J. Geophys. Res., 114, C01002, doi:10.1029/2008JC0048682009, 2009.

Thorpe, S. A.: Recent developments in the study of ocean turbulence, Annu. Rev. Earth Pl. Sc., 32, 91–109, 2004.

Uematsu, M., Duce, R. A., and Prospero, J. M.: Deposition of atmospheric mineral particles in the North Pacific ocean, J. Atmos. Chem., 3, 123–138, 1985.

Venchiarutti, C., Jeandel, C., and Roy-Barman, M.: Particle dynamics in the wake of Kerguelen Island traced by thorium isotopes (Southern Ocean, KEOPS program), Deep-Sea Res. Pt. I, 55, 1343–1363, 2008.

Wallace, D. W. R. and Moore, R. M.: Vertical profiles of CC13F (F-11) and CC12F (F-12) in the central Arctic Ocean basin, J. Geophys. Res., 90, 1155–1166, 1985.

Yanagimoto, D. and Kawabe, M.: Deep-circulation flow at midlatitude in the western North Pacific, Deep-Sea Res. Pt. I, 54, 2067–2081, 2007.